during the microtoming process. The results from TEM and WAXS, however, are in good agreement, notably in the case of diblock copolymers where narrow distribution of cluster sizes were observed. By SAXS, the Bessel function fit of the profile may only provide a lower bound on cluster size, analogous to the fit of the spherical microdomains in sample S. We found that the cluster size estimated by this technique for sample C was actually bigger compared to the size estimated by TEM (Table I). In the case of the homopolymers, a fit of the Percus-Yevick/Bessel function formulation could not be obtained.

As mentioned in the Introduction, it is desirable to have a uniform distribution of clusters in the composite material. Whether or not the clusters formed in the block copolymers could be said to be "uniformly distributed" depends upon the length scale examined. Within the microdomains, the clusters appeared to be uniformly, albeit randomly, distributed. However, as the length scale of consideration is increased to the d spacing of the material, the cluster distribution would have the form of a step function and not a uniform distribution. As the length scale is increased to bulk dimensions, inhomogeneities seen in the microdomains are averaged out by the various orientations of sections of the microdomains. It would be interesting to obtain samples with macroscopically well-ordered metal cluster-containing cylindrical or lamellar morphology since they would display anisotropic properties.

Conclusion

The two organometallic monomers presented herein provide a relatively straightforward method of synthesizing palladium and platinum nanoclusters within a nonconductive polymeric matrix. They cleanly undergo ROMP with a well-defined metal alkylidene initiator to give homopolymers or diblock copolymers with the desired composition that are stable and tractable. The block copolymers exhibit microphase separation with morphologies that are consistent with their compositions. Reduction of the metal complexes in the solid polymer films under relatively mild conditions affords clusters in the range 20–125 Å in diameter (a size which depends on the nature of the polymer) that are metallic in nature, according to X-ray studies. The microphase-separated morphology of the block copolymers provided enhanced kinetic control of the cluster formation process, effectively eliminating cluster aggregation into larger particles observed in the reduced organometallic homopolymers. Extended heating of cluster-containing films did not result in excessive aggregation of these small clusters. Further syntheses and annealing studies are planned in order to explore this kinetic limitation.

The diblock approach is effective if small clusters with a narrow size distribution are desired. The small dimensions of the metal-containing microdomains appear to limit cluster size. The studies reported here should be compared with related studies concerning the preparation of gold and silver clusters in block copolymers.[38] It also now seems possible to grow a single cluster within a spherical microdomain, the ultimate control in cluster growth and size.[61] Research to examine the dielectric and nonlinear optical properties of these cluster-containing composite materials is in progress.

Acknowledgment. We thank the National Science Foundation (Grant DMR 87-19217 through the MIT Center for Material Science and Engineering) and Nippon-Zeon for financial support. The B.F. Goodrich Co. is acknowledged for a generous supply of MTD. Helpful discussions with C. C. Cummins and a gift of $Li(Cp^N)$ from him are appreciated. G.S.W.C. acknowledges the NSF for a Graduate Fellowship.

Registry No. $Mo(CHCMe_2Ph)(NAr)(O\text{-}t\text{-}Bu)_2$, 126949-65-3; $W(CH\text{-}t\text{-}Bu)(NAr)(O\text{-}t\text{-}Bu)_2$, 107440-84-6; $Pd(Cp^N)(PA)$, 141483-81-0; $LiCp^N$, 141485-36-1; $[Pd(PA)Cl]_2$, 12131-44-1; $Pt(Cp^N)Me_3$, 141483-86-5; $[PtMe_3I]_4$, 18253-26-4; $[Pd(Cp^N)(PA)]_n$, 141483-82-1; $[Pt(Cp^N)Me_3]n$, 141483-84-3; [Pd]50[MTD]113, 141483-85-4; [Pt]40[MTD]200, 141483-87-6.

(61) Ng Cheong Chan, Y., unpublished results.

Protonated Pentatitanate: Preparation, Characterizations, and Cation Intercalation

Takayoshi Sasaki,* Yu Komatsu, and Yoshinori Fujiki

National Institute for Research in Inorganic Materials, 1-1 Namiki, Tsukuba, Ibaraki 305, Japan

Received March 3, 1992. Revised Manuscript Received May 18, 1992

A protonated pentatitanate with a monoclinic layer structure, $H_2Ti_5O_{11}\cdot 3H_2O$, has been prepared by treating its parent compound, $Cs_2Ti_5O_{11}$, with a hydrochloric acid solution. The hydration water, as well as protons, is introduced upon interlayer Cs ion removal, expanding the separation between lost lamellae, $[Ti_5O_{11}^{2-}]_\infty$. Half of the substituting protons exist as oxonium ions and the other half as hydroxyl groups, both of which are reversibly exchangeable with cations. The material lost free interlayer water up to 100 °C yielding a less hydrated phase, $H_2Ti_5O_{11}\cdot H_2O$, with a smaller interlayer distance. Subsequent dehydration resulted in the metastable form of titanium dioxide TiO_2(B) around 500 °C, which was transformed into anatase and then rutile at elevated temperatures. The material $H_2Ti_5O_{11}\cdot 3H_2O$ underwent a stepwise intercalation reaction with K and Cs ions, replacing oxonium ions and hydroxylated protons in this order. This reaction gave rise to half- and fully-loaded phases with different degrees of swelling. The structural characterizations of the phases indicate that the reaction proceeds topochemically, accompanied by a lateral gliding of adjacent host lamellae along the c axis as well as a swelling/contraction of the interlayer spacing.

Introduction

There are a series of layered titanates with the general formula $M_2O\cdot nTiO_2$ (where M denotes alkali-metal ions). The crystal structures are composed of host lamellae and charge-compensating interlayer cations, as shown schematically in Figure 1. The following members are ca-

0897-4756/92/2804-0894$03.00/0

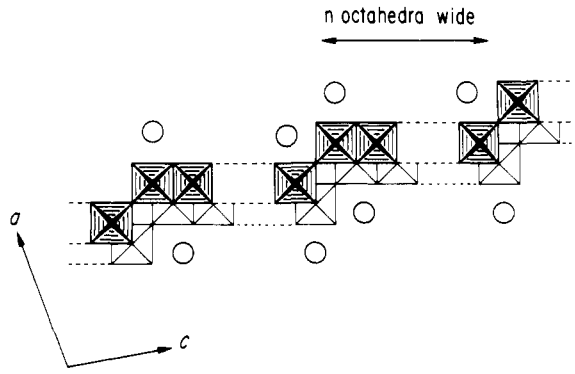

Figure 1. Schematic description of the structure feature for layered titanates $M_2O{\cdot}nTiO_2$ (M: alkali metals). Projection along the b axis. The hatched TiO_6 octahedra are at $y = {}^1/_2$ and the others at $y = 0$. The octahedra are combined by sharing edges making a block of n octahedra wide. The block is connected with other blocks at a distance $b/2$ above and below to form a zigzag ribbon elongating parallel to the b axis. The ribbon is then linked with other ribbons having their apexes common to produce a corrugated lamella. The lamellae are stacked along the a axis, holding univalent cations (expressed as the circles) between them.

talogued in the family: trititanate, $Na_2Ti_3O_7$ ($n = 3$);[1] tetratitanate, $K_2Ti_4O_9$ ($n = 4$);[2,3] pentatitanate, $Cs_2Ti_5O_{11}$ ($n = 5$).[4,5] The layer sequence is AAA for the trititanate, offering a trigonal prismatic cavity for Na ions. On the other hand, the other members accommodate K and Cs ions in pseudo-cubic sites produced by stacking the layers with a $b/2$ translation (ABA mode).

It has been established that the tri- and tetratitanates can be protonated preserving the layer structures.[6-8] The resulting protonated forms of the layered titanates, $H_2Ti_3O_7$ and $H_2Ti_4O_9{\cdot}1.2H_2O$, show prominent intercalation chemistry. These two types of protonated titanates exhibit distinct characteristics which play an important role in determining the intercalation capabilities; $H_2Ti_3O_7$ possesses a dehydrated interlayer environment with a short separation, while $H_2Ti_4O_9{\cdot}1.2H_2O$ has a rather open interlayer space holding waters of hydration. Fundamental studies have been conducted, for example, on the preparation of organic–inorganic complexes[9-11] and on the reaction mechanism of cation intercalation processes.[8,12-17] These layered titanates have also attracted considerable attention from a variety of practical standpoints such as sorptions, separations and solidification/immobilization of radioactive nuclides.[18-24] In addition, recent successes in deriving alumina-pillared microporous materials from these titanates have widened their scope for catalysts, catalyst supports, and molecular sieves.[25,26]

It is anticipated that a protonated pentatitanate will show distinctive properties in relation to those for $H_2Ti_3O_7$ and $H_2Ti_4O_9{\cdot}1.2H_2O$. Thus it is of interest to attempt a protonation of the pentatitanate and to examine its intercalation properties in terms of the differences in structural features. This paper describes the synthesis and characterizations of the protonated pentatitanate. The K and Cs ion intercalation processes are studied and discussed on the basis of the structural data.

Experimental Section

Reagents and Materials. The titanium dioxide used was of 99.98% purity (Rare Metallic, Co. Ltd., rutile form). All the other chemicals were of 99.9% purity or higher and were used without further purification. Distilled deionized water was used throughout the experiments.

The cesium pentatitanate $Cs_2Ti_5O_{11}$ was prepared by using a procedure similar to that reported previously.[4] Starting reagents of Cs_2CO_3 and TiO_2 (1:4.5 molar ratio) were ground intimately in an Ar-filled glovebox and heated 800 °C for 1 h to be decarbonated. Then the mixtures were ground again, followed by calcination at 1000 °C for 20 h. The resulting product, cooled in an ambient atmosphere, was identified by powder X-ray diffraction (XRD) technique to be a hydrated form of cesium pentatitanate $Cs_2Ti_5O_{11}{\cdot}(1+x)H_2O$ ($0.5 < x < 1$).[4] Amorphous substances such as Cs_2O, CsOH, and Cs_2CO_3 could be present based on the composition of the starting mixtures. Due to an evaporative loss of the Cs component at the calcination temperature, starting from a stoichiometric system, yielded not a single phase of $Cs_2Ti_5O_{11}$ but a Cs-poorer compound, $Cs_xTi_{2-x/4}\square_{x/4}O_4$ ($x \sim 0.70$; $\square$, vacancy),[27] as well as $Cs_2Ti_5O_{11}$.

Protonation. The extraction of interlayer Cs ion was attempted by treating a weighed amount of the calcined product above with a 1 mol dm^{-3} HCl solution at room temperature. The solution to solid ratio was 100 cm^3 g^{-1}. The solution was replaced every 24 h, which was repeated three times. The amorphous impurities could be eliminated by this treatment. Then the excessive acid was washed with water until the pH value of the supernatant was between 5 and 6. The resulting solid was dried over a saturated NaCl solution (relative humidity 70%) to a constant weight.

Equilibrations. The intercalation of K and Cs ions was examined by titrating the protonated form of pentatitanate in a batchwise technique: 0.2 g of the material was equilibrated with 20 cm^3 of MCl–MOH aqueous solution (M = K, Cs) at 25 ± 0.5 °C for 7 days. The ionic strength of the solution was adjusted to 0.1, and the ratio of solute chloride and hydroxide was changed from 0.1/0.0 to 0.0/0.1. After the equilibration, aliquots of the supernatant solutions were pipetted and analyzed for their pH values and cation contents. The cation uptake was deduced from a difference between the initial and residual concentrations of

(1) Andersson, S.; Wadsley, A. D. *Acta Crystallogr.* **1961**, *14*, 1245.
(2) Verbaere, A.; Tournoux, M. *Bull. Soc. Chim. Fr.* **1973**, 1237.
(3) Dion, M.; Piffard, Y.; Tournoux, M. *J. Inorg. Nucl. Chem.* **1978**, *40*, 917.
(4) Grey, I. E.; Madsen, I. C.; Watts, J. A.; Bursill, L. A.; Kwiatkowska, J. *J. Solid State Chem.* **1985**, *58*, 350.
(5) Kwiatkowska, J.; Grey, I. E.; Madsen, I. C.; Bursill, L. A. *Acta Crystallogr.* **1987**, *B43*, 258.
(6) Marchand, R.; Brohan, L.; Tournoux, M. *Mater. Res. Bull.* **1980**, *15*, 1129.
(7) Izawa, H.; Kikkawa, S.; Koizumi, M. *J. Phys. Chem.* **1982**, *86*, 5023.
(8) Sasaki, T.; Watanabe, M.; Komatsu, Y.; Fujiki, Y. *Inorg. Chem.* **1985**, *24*, 2265.
(9) Clément, P.; Marchand, R. *C. R. Acad. Sci. Paris. Ser. II* **1983**, *296*, 1161.
(10) Izawa, H.; Kikkawa, S.; Koizumi, M. *Polyhedron* **1983**, *2*, 741.
(11) Miyata, H.; Sugawara, Y.; Kuroda, K.; Kato, C. *J. Chem. Soc., Faraday Trans. 1* **1988**, *84*, 2677.
(12) Marchand, R.; Brohan, L.; M'bedi, R.; Tournoux, M. *Rev. Chim. Mineral.* **1985**, *21*, 476.
(13) Tournoux, M.; Marchand, R.; Brohan, L. *Prog. Solid State Chem.* **1986**, *17*, 33.
(14) Izawa, H.; Kikkawa, S.; Koizumi, M. *Yogyo Kyokaishi* **1986**, *94*, 621.
(15) Sasaki, T.; Watanabe, M.; Komatsu, Y.; Fujiki, Y. *Bull. Chem. Soc. Jpn.* **1985**, *58*, 3500.
(16) Sasaki, T.; Komatsu, Y.; Fujiki, Y. *Mater. Res. Bull.* **1987**, *22*, 1321.
(17) Sasaki, T.; Komatsu, Y.; Fujiki, Y. *Inorg. Chem.* **1989**, *28*, 2776.
(18) Izawa, H.; Kikkawa, S.; Koizumi, M. *J. Solid State Chem.* **1985**, *60*, 264.
(19) Izawa, H.; Kikkawa, S.; Koizumi, M. *J. Solid State Chem.* **1987**, *69*, 336.
(20) Komatsu, Y.; Fujiki, Y.; Sasaki, T. *Bunseki Kagaku* **1982**, *31*, E225.
(21) Komatsu, Y.; Fujiki, Y.; Sasaki, T. *Bunseki Kagaku* **1983**, *32*, E33.
(22) Sasaki, T.; Komatsu, Y.; Fujiki, Y. *Sep. Sci. Technol.* **1983**, *18*, 49.
(23) Sasaki, T.; Komatsu, Y.; Fujiki, Y. *J. Radioanal. Nucl. Chem.* **1986**, *107*, 111.
(24) Fujiki, Y.; Komatsu, Y.; Sasaki, T.; Ohta, N. *Nippon Kagaku Kaishi* **1981**, 1656.
(25) Cheng, S.; Wang, T. *Inorg. Chem.* **1989**, *28*, 1283.
(26) Anderson, M. W.; Klinowski, J. *Inorg. Chem.* **1990**, *29*, 3260.
(27) Grey, I. E.; Li, C.; Madsen, I. C.; Watts, J. A. *J. Solid State Chem.* **1987**, *66*, 7.

Table I. Powder XRD Data for $H_2Ti_5O_{11}\cdot 3H_2O$

h k l	d_{calcd}, Å	d_{obsd}, Å	intensity
0 0 1	13.37	13.38	3
2 0 0	10.42	10.41	100
2 0 $\bar{2}$	7.36	7.36	<1
2 0 1	6.84	6.83	10
4 0 0	5.21	5.21	3
2 0 $\bar{3}$	5.01	5.00	<1
2 0 2	4.73	4.73	3
4 0 $\bar{3}$	4.57	4.57	<1
0 0 3	4.46	4.46	<1
4 0 1	4.24	4.24	<1
6 0 $\bar{1}$	3.813	3.816	<1
1 1 0	3.690	3.689	5
2 0 3	3.553	3.554	1
6 0 0	3.474	3.472	1
3 1 0	3.300	3.299	7
3 1 1	3.053	3.049	4
2 0 $\bar{5}$	2.933	2.931	6
5 1 0	2.788	2.786	1
8 0 $\bar{4}$	2.753	2.753	2
0 0 5	2.674	2.675	4
5 1 1	2.577	2.577	<1
5 1 $\bar{4}$	2.560	2.562	<1
8 0 $\bar{5}$	2.531	2.530	1
2 0 $\bar{6}$	2.417	2.417	1
8 0 1	2.363	2.363	<1
10 0 $\bar{3}$	2.343	2.342	2
3 1 $\bar{5}$	2.341		
10 0 $\bar{4}$	2.303	2.304	3
0 0 6	2.229	2.229	4
10 0 $\bar{5}$	2.202	2.202	1
9 1 $\bar{1}$	2.069	2.070	<1
2 0 6	2.001	2.001	5
9 1 $\bar{5}$	2.000		
12 0 $\bar{4}$	1.948	1.948	3
12 0 $\bar{3}$	1.947		
10 0 1	1.930	1.929	2
12 0 $\bar{5}$	1.908	1.908	<1
12 0 $\bar{2}$	1.907		
0 2 0	1.875	1.876	3
2 2 0	1.845	1.846	3
2 2 1	1.808	1.807	<1
3 1 6	1.685	1.686	2
10 0 3	1.625		
13 1 $\bar{4}$	1.624	1.624	2
9 1 $\bar{8}$	1.623		
2 2 $\bar{5}$	1.580	1.579	<1

the solution, which was determined by a Hitachi 180-80 atomic absorption spectrometer. The solid phases, conditioned at a relative humidity of 70%, were allowed to characterizations.

Chemical Analysis. The HCl-treated product and some of K and Cs ion intercalated materials were analyzed with a wet method as follows: A weighed amount of the material (~200 mg) was decomposed by a mixed acid solution (10 cm^3 of 1/1 H_2SO_4 + 5 cm^3 of 1/1 HF) at 160 °C in an autoclave vessel. The cations were determined by atomic absorption spectrometry and Ti by gravimetry using a cupferron as a precipitant. The water content was estimated from the weight loss at 800 °C.

Apparatus. The powder XRD patterns were obtained by a Rigaku Denki RAD-2B diffractometer using graphite-monochromatized Cu Kα radiation (λ = 1.5405 Å). Cell parameters were refined by a least-squares technique[28] for the data collected over the 2θ range 3–60° at a step-scan speed of 0.3° min^{-1}.

The IR spectra were recorded on a sample pelletized with KBr with a Hitachi EPI-G3 grating infrared spectrometer.

The differential thermal analysis and thermogravimetry data were obtained by a Rigaku Denki TAS 100 thermal analyzer at a heating rate of 10 °C min^{-1}.

(28) Appleman, D. E.; Evans, H. T., Jr. Report No. PB216188, U. S. Dept. of Commerce, National Technical Information Service, Springfield, VA, 1973.

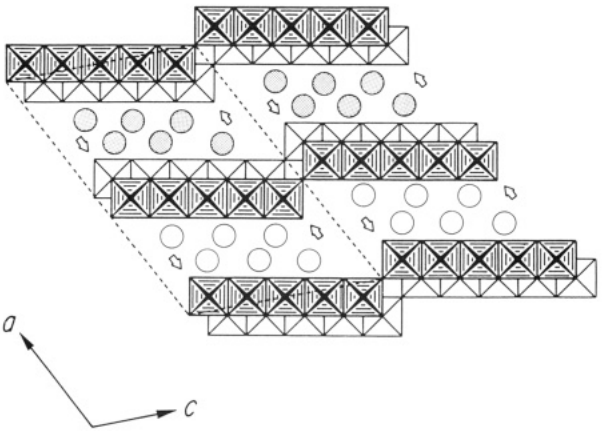

Figure 2. Idealized representation of the structure for the protonated pentatitanate $H_2Ti_5O_{11}\cdot 3H_2O$. The arrows point at the possible oxygen atoms to be hydroxylated. The open and stippled circles represent H_2O(or H_3O^+) at y = 0 and $^1/_2$, respectively. (Their configuration is tentative.)

Results and Discussion

Formation of Protonated Pentatitanate. The titanate retained its crystallinity during the acid treatment. The XRD data for the HCl-treated product can be indexed as shown in Table I in a *C*-base-centered monoclinic lattice ($C2/m$, Z = 4), which is identical to that for its parent material $Cs_2Ti_5O_{11}$. The refined cell parameters are a = 23.431 (4) Å, b = 3.749 (1) Å, c = 15.029 (3) Å, and β = 117.16 (2)°, where the numerals in parentheses correspond to the standard deviation in the last digit. The comparison of these values with the lattice constants for $Cs_2Ti_5O_{11}$ [a = 19.719 (8) Å, b = 3.808 (1) Å, c = 15.023 (6) Å, β = 106.93 (3)°][4] indicates the following structural modifications on the HCl treatment:

(i) The host framework of $[Ti_5O_{11}^{2-}]_\infty$ remained unchanged.

(ii) The stacking mode of ABA was preserved.

(iii) The interlayer spacing (=$(a/2)\sin\beta$) expanded from 9.4 to 10.4 Å.

(iv) A relative configuration of the adjacent host lamellae was changed by their glide of approximately one-octahedron width (~3 Å) along the c axis.

The chemical analysis on the HCl-treated product gave 0.9 wt % for Cs_2O, 83.9 wt % for TiO_2, and 15.2 wt % for H_2O. This means that almost all of Cs ions (over 99%) initially accommodated in the interlayer space were extracted.

The above observations lead to the conclusion that a protonated pentatitanate with a layer structure is yielded according to the following equation:

$$Cs_2Ti_5O_{11}(s) + 2H^+(aq) + 3H_2O(aq) \rightarrow H_2Ti_5O_{11}\cdot 3H_2O(s) + 2Cs^+(aq)$$

Figure 2 shows the idealized representation of the structure for $H_2Ti_5O_{11}\cdot 3H_2O$ in projection along the b axis. The material is characterized by its large interlayer spacing, high degree of hydration, and large free area per negative charge of the host lamellae, compared with three types of protonated titanates reported so far; $H_2Ti_3O_7$ [7.9 Å],[7] $H_2Ti_4O_9\cdot 1.2H_2O$ [9.1 Å],[6-8] and $H_xTi_{2-x/4}\square_{x/4}O_4\cdot H_2O$ [9.4 Å][29] (for $x \sim 0.70$). The numerals in square brackets denote the interlayer distance. The last material is not classified as the structural relative in Figure 1 but is related to the layered structure for lepidocrocite, FeO(OH).[30]

(29) Sasaki, T.; Komatsu, Y.; Fujiki, Y. *J. Chem. Soc., Chem. Commun.* **1991**, 817.

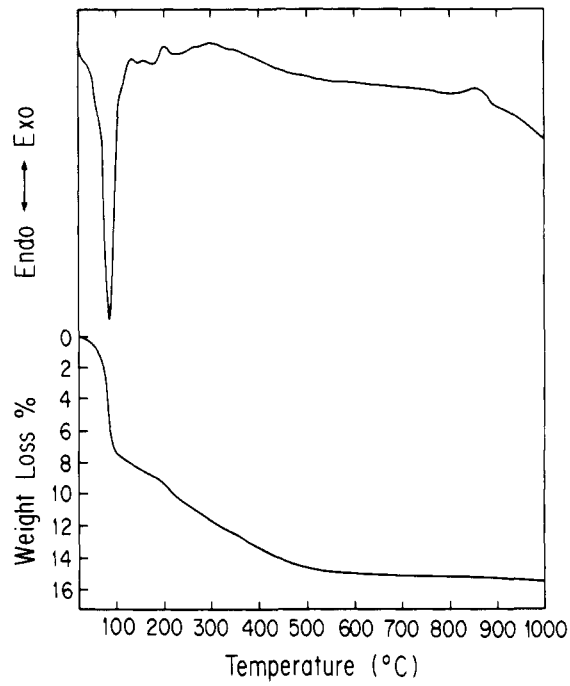

Figure 3. Differential thermal analysis and thermogravimetric curves for $H_2Ti_5O_{11}\cdot 3H_2O$. Heating rate 10 °C min^{-1}.

The chemical composition, $H_2Ti_5O_{11}\cdot 3H_2O$, indicates that six water molecules are accommodated in a unit interlayer space encircled by a pair of the block $Ti_{10}O_{22}^{4-}$ (which corresponds to half the unit cell). The restriction of the available space makes it difficult to arrange six molecules in a straight line along the *c* axis. Some zigzag configuration (see Figure 2) is likely to occur, which gives the expansion of interlayer spacing by 1.0 Å despite the Cs ion removal.

The nonsharing oxygen atoms in the framework, designated by arrows in Figure 2, are presumably hydroxylated due to their higher electronegativities. The unit lattice contains four nonsharing oxygen atoms while eight protons are introduced in place of Cs ions. The remaining four protons may be in the form of oxonium ions in the interlayer space.

Two kinds of protonic species are reflected in the IR data, which shows three absorption bands, 3650–2500 cm^{-1} centered at 3400 cm^{-1}, 1720–1550 cm^{-1} centered at 1630 cm^{-1}, and 1050–920 cm^{-1} centered at 970 cm^{-1}. According to Ryskin,[31] these three can be assigned to O–H stretching mode for interlayer water, oxonium ions and hydroxyl groups, H–O–H bending for water and oxonium ions, and O–H bending for hydroxyls, respectively.

Dehydration of Protonated Pentatitanate. The pentatitanate $H_2Ti_5O_{11}\cdot 3H_2O$ lost water in two steps, as shown in Figure 3, although they were not well resolved: (1) A rapid loss in the temperature range 40–100 °C accompanying a sharp endotherm, and (2) a gradual process in 100–500 °C, which amounted to 7.7 and 7.5 wt %, respectively. Figure 4 illustrates powder XRD patterns of the material which was heated at elevated temperatures (100–1000 °C at an interval of 100 °C) for 1 h. A dehydrated intermediate obtained after heating at 100 °C held a good quality of crystallinity, indicative of a well-ordered structure. Its X-ray data was indexed in terms of a *C*-base-centered cell [a = 20.005 (5) Å, b = 3.763 (1) Å, c = 14.998 (8) Å, β = 124.01 (2)°],[32] which indicates a topotactic shrinkage of the interlayer separation (~2.1 Å) upon water loss. This phase was fairly stable. Neither exposure to an atmospheric humidity nor immersion in water caused it to revert to the original swelled phase.

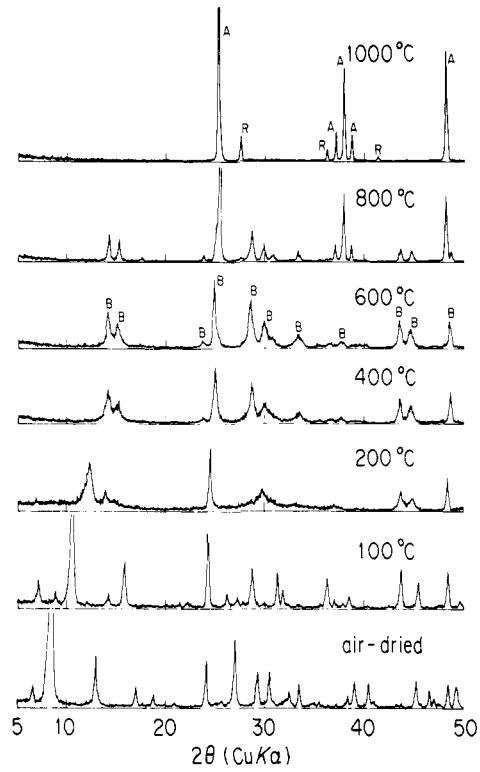

Figure 4. Powder XRD patterns in the dehydration process for $H_2Ti_5O_{11}\cdot 3H_2O$. Heating time 1 h. B, TiO_2(B); A, anatase; R, rutile.

The chemical composition $H_2Ti_5O_{11}\cdot 3H_2O$ is reformulated as $(H_3O)\cdot(2H_2O)\cdot Ti_5O_{10}(OH)$, in line with the discussion on the crystal structure. It is reasonably presumed that free interlayer water was evaporated up to 100 °C forming the material of a composition $H_2Ti_5O_{11}\cdot H_2O$. Note that 2 mol of water/formula weight corresponds to 7.6 wt %, which coincides well with the observed loss in the first step. The degree of hydration is similar to that of the protonated tetratitanate $H_2Ti_4O_9\cdot 1.2H_2O$.[6-8]

In the temperature range above 100 °C, charge-bearing species began to leave the structure requiring a rearrangement of the framework, which was manifested by the loss of crystallinity in Figure 4. The completely dehydrated material crystallized into the metastable form of titanium dioxide, TiO_2(B) (see the patterns for 400 and 600 °C), that was characterized by the Freudenbergite type structure.[33] It has been reported that this metastable phase is also formed by dehydrating the protonated tetratitanate $H_2Ti_4O_9\cdot 1.2H_2O$.[6,12,13] The refined cell parameters [a = 12.16 (1) Å, b = 3.741 (4) Å, c = 6.507 (9) Å, β = 106.8 (1)°] agree well with those for TiO_2(B) obtained from $H_2Ti_4O_9\cdot 1.2H_2O$. The broad exothermic peak in the temperature range 200–400 °C may be due to the overlapping a crystallization exotherm and a dehydration endotherm. A relatively sharp peak at 180 °C may be correlated with a conversion from $H_2Ti_5O_{11}\cdot H_2O$ to a precursor phase of TiO_2(B) (see the XRD pattern at 200 °C). In the temperature range 800–900 °C, the metastable TiO_2(B) was transformed into anatase, which was then changed into

(30) Reid, F. M.; Mumme, W. G.; Wadsley, A. D. *Acta Crystallogr.* **1968**, *B24*, 1228.
(31) Ryskin, Y. I. *The Infrared Spectra of Minerals*; Farmer, V. C., Ed.; Mineralogical Society: London, 1974; p 137.
(32) Indexed XRD data are deposited as supplementary material.
(33) Ishiguro, T.; Tanaka, K.; Marumo, F.; Ismail, M. G. M. U.; Somiya, S. *Acta Crystallogr.* **1978**, *B34*, 255.

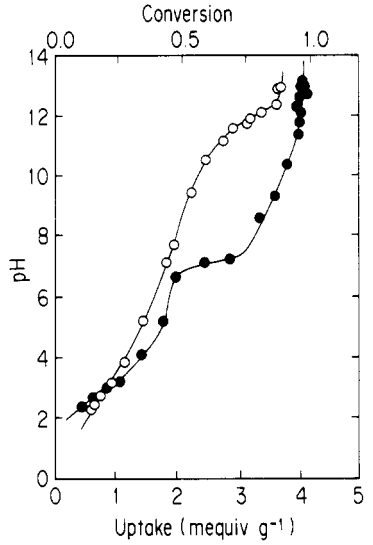

Figure 5. Cation uptake curves as a function of equilibrium pH. (●) K, (○) Cs, solid, 0.2 g; $H_2Ti_5O_{11}\cdot 3H_2O$; titrant, 0.02 dm^3 of (MCl–MOH), M = K, Cs; ionic strength, 0.1; temperature; 25 ± 0.5 °C.

rutile, corresponding to the exothermic peak around 870 °C in the DTA curve (see Figure 3).

The phase change driven by the heat treatment can be summarized as follows:

$$H_2Ti_5O_{11}\cdot 3H_2O \xrightarrow[100\ °C]{} H_2Ti_5O_{11}\cdot H_2O \xrightarrow[400\ °C]{}$$
$$[10.4\ Å] \qquad [8.3\ Å]$$
$$TiO_2(B) \rightarrow \text{anatase} \xrightarrow[800\text{–}1000\ °C]{} \text{rutile}$$

where the numerals in brackets refer to the interlayer distances (=d_{200}).

Cation Intercalation Behavior. The protonated pentatitanate $H_2Ti_5O_{11}\cdot 3H_2O$ was titrated with K and Cs ions (see Figure 5) in order to examine its intercalation properties. The uptake curves indicate the following three points;

(i) The apparent saturated capacity for K and Cs were 4.1 and 3.7 mequiv g^{-1}, respectively. A nearly reversible exchange was accomplished with the K ion: The exchangeable protons are theoretically estimated at 4.24 mequiv g^{-1} on the basis of the stoichiometry $H_2Ti_5O_{11}\cdot 3H_2O$.

(ii) The material is a bifunctional solid acid. The curves had an inflection point of around 50% conversion (the loading level of 2 mequiv g^{-1}), although this was not well defined for the Cs ion.

(iii) The material preferred the Cs ion to the K ion at an early stage (below the loading level of 0.7 mequiv g^{-1}) whereas the contrary was the case at a higher loading range. This phenomenon can be understood as follows: The hydration energy of cations plays one of the most important roles in determining their incorporation preference because aquo ions are required to strip some or all of their hydrated water when diffusing into host lattices. Since the Cs ion interacts with water molecules less strongly than the K ion, the former is preferred at an early stage. On the other hand, as the interlayer space begins to be filled with the cations, steric constraints may become significant, which overcomes the contribution from the hydration terms and reverts incorporation acidities.

Reaction Scheme. The Cs incorporation reaction can be interpreted as a two-stage process by monitoring the structural changes of the solid phases with the XRD techniques (see Figure 6), which is consistent with the bifunctional nature pointed out above. Two immiscible

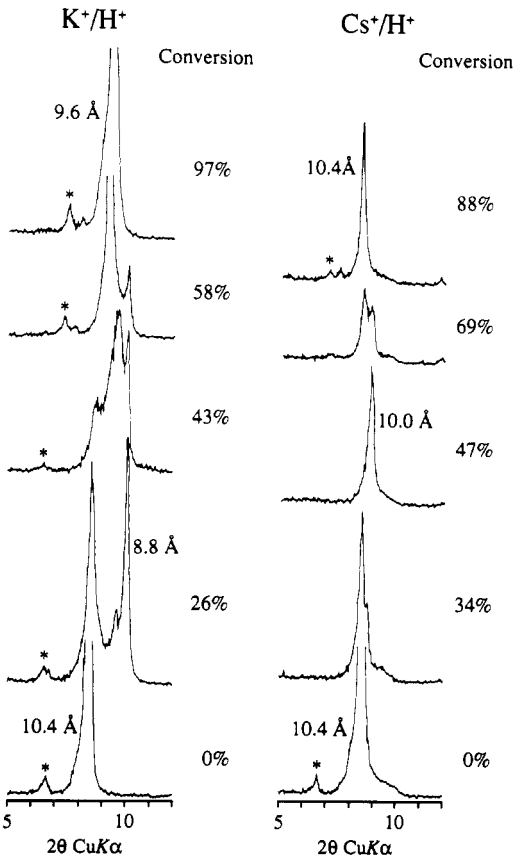

Figure 6. Powder XRD patterns in the K and Cs intercalation processes. The numerals represent the conversion level. The angular region where (200) reflections corresponding to interlayer distance occur is focused. The reflection with an asterisk is from the (001) plane.

solid phases, characterized by interlayer distances of 10.4 and 10.0 Å, were found in the conversion range 0–50%. The former declined as the reaction proceeded and eventually disappeared at 50% conversion, where the latter phase was predominant. Thus the phases are assigned as the starting titanate $H_2Ti_5O_{11}\cdot 3H_2O$ (designated as phase HH) and as a half-loaded phase (phase CsH). A discontinuous change in the interlayer distance was also observed beyond 50% conversion where phase CsH was converted into a swelled phase (phase CsCs, d_{200} = 10.4 Å). This phase was present alone near the end point of the titration. It is to be pointed out that the phases which appeared in the incorporation process showed a considerably wide range of miscibility. Thus phase CsCs, in which 88% of exchangeable protons were consumed, is likely to be in the solubility range of a fully loaded phase. This is supported from a close matching in cell dimensions of phase CsCs (described below) and a hydrated form of the cesium pentatitanate $Cs_2Ti_5O_{11}\cdot(1+x)H_2O$ reported by Grey et al.[4]

The K intercalation process can be basically understood in a manner similar to that for the Cs process although the XRD patterns, depicted in Figure 6, showed some complexity. In the conversion range 0–50%, a new phase with an interlayer distance of 8.8 Å (phase KH) was evolved besides phase HH. A broad peak also occurred, as phase HH diminished, in an intermediate angular region of (200) reflections from phase HH and KH, which appears to suggest another phase. However, the following inference may give a reasonable interpretation: The diffuse reflection of spacing 9.1–9.2 Å may be ascribed to a mixed layer stacking of two kinds of spacings, 10.4 Å for phase HH and 8.8 Å for phase KH. The phenomenon may be associated with the paracrystalline nature of the pentatitanate, as

Table II. Unit-Cell Dimensions for the Cation-Loaded Phases[a]

phase	a, Å	b, Å	c, Å	β, deg
HH	23.431 (4)	3.749 (1)	15.029 (3)	117.16 (2)
KK	23.326 (6)	3.784 (1)	14.907 (5)	125.14 (2)
CsH	21.407 (6)	3.763 (1)	14.995 (5)	111.07 (3)
CsCs	25.087 (5)	3.770 (1)	14.970 (4)	123.18 (2)

[a] Estimated standard deviations in the last figure are given in parentheses.

pointed out by Bursill et al.,[34] which facilitates the introduction of some defects. Phase KH and the interstratified material changed into a good crystalline phase (phase KK, d_{200} = 9.6 Å) in the latter half of the process. Phase KH may be a half-loaded phase, although its isolation was unsuccessful due to the coexistence of mixed layers as well as phase KK even at 50% conversion.

To sum up the data on the titration behavior and structural changes, the K and Cs ion intercalation processes can be formulated in terms of the following stepwise scheme:

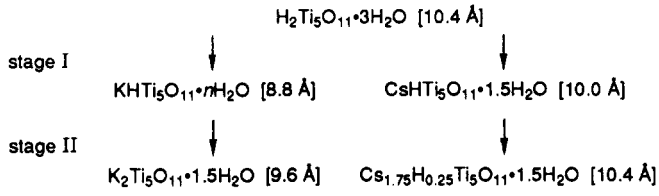

The number of water molecules per formula weight decreased from 3.0 to 1.5 in stage I, while it was kept unchanged in stage II. (The water content, n, for phase KH would be approximately 1.5 because a titrated product at the proton consumption of ~50% had the corresponding water loss although its was heterogeneous.) This phenomenon strongly suggests the following reaction mechanism: Incorporated cations substituted with oxonium ions, simultaneously ejecting some interlayer water in stage I, and then with hydroxylated protons in stage II. The compositional change is consistent with the structural model for $H_2Ti_5O_{11}\cdot 3H_2O$ in which two kinds of exchangeable protonic species, oxonium ions and hydroxyls, are accommodated in equal amount.

The XRD data for the obtained phases can be indexed in the C-base-centered monoclinic lattice,[35] proving that the ABA stacking sequence is preserved throughout the processes. The lattice constant refinements (summarized in Table II) indicate that the cation incorporation gives rise to an expansion/shrinkage of the host lamella separation and a gliding of the lamellae along the c axis.

It is of interest to compare the cation intercalation behavior in $H_2Ti_5O_{11}\cdot 3H_2O$ with that in the protonated tetratitanate $H_2Ti_4O_9\cdot 1.2H_2O$. Both of the protonated titanates showed similar acidities toward the cations except for the surpassing capacity for the latter (5.57 mequiv g^{-1}). The latter titanate undergoes a stepwise intercalation forming $n/4$ (n = 1, 2, 3, 4) loaded phases.[8,15-17]

Two types of arrangement of interlayer species have been demonstrated on the basis of structural characterizations of the solid phases appearing in the intercalation processes with $H_2Ti_4O_9\cdot 1.2H_2O$:[8,17] The monolayer configurations of cations and water molecules when the interlayer cation content is low (generally below $^1/_2$ conversion) and the unique bilayer arrangements for higher contents of cations ($>^3/_4$ conversion). The formation of the bilayer is considered to be driven by the need to make a cation–cation distance larger. Taking the magnitude of the interlayer spacings into consideration, it is likely that the phases evolved from $H_2Ti_5O_{11}\cdot 3H_2O$ possess monolayer arrangements. Actually the structural refinement on the cesium pentatitanate hydrate $Cs_2Ti_5O_{11}\cdot(1+x)H_2O$, isomorphous with phase CsCs, revealed a monolayer configuration of Cs ions and H_2O molecules.[5] It may not be necessary to make a bilayer configuration of interlayer species even at a high cation content because the commodious interlayer space, wider by one-octahedron width than that in $H_2Ti_4O_9\cdot 1.2H_2O$, could avoid a close contact of the cations.

Supplementary Material Available: Tables of powder XRD data for $H_2Ti_5O_{11}\cdot H_2O$, phase KK, phase CsH, and phase CsCs (8 pages). Ordering information is given on any current masthead page.

(34) Bursill, L. A.; Smith, D. J.; Kwiatkowska, J. *J. Solid State Chem.* **1987**, *69*, 360.

(35) Deposited as supplementary material.